Discovering host protein interactions specific for SARS-CoV-2 RNA genome

Roberto Giambruno[1,2,#,$], Elsa Zacco[3,#], Camilla Ugolini[1,#], Andrea Vandelli[4,5], Logan Mulroney[1,6], Manfredi D'Onghia[1], Elena Criscuolo[7], Matteo Castelli[7], Nicola Clementi[7,8], Massimo Clementi[7,8], Nicasio Mancini[7,8], Tiziana Bonaldi[9,10], Stefano Gustincich[3], Tommaso Leonardi[1], Gian Gaetano Tartaglia[3,11,$] and Francesco Nicassio[1,$]

1. Center for Genomic Science of IIT@SEMM, Fondazione Istituto Italiano di Tecnologia, 20139 Milano, Italy.
2. Institute of Biomedical Technologies, National Research Council, 20090 Segrate, Italy.
3. Center for Human Technologies, Istituto Italiano di Tecnologia, Genoa, Italy
4. Department of Biochemistry and Molecular Biology, Universitat Autònoma de Barcelona, Bellaterra, 08193 Barcelona, Spain
5. Universitat Pompeu Fabra (UPF), 08003 Barcelona, Spain
6. European Molecular Biology Laboratory, European Bioinformatics Institute, Hinxton, UK
7. Laboratory of Microbiology and Virology, Vita-Salute San Raffaele University; via Olgettina 58, 20132 Milan, Italy.
8. Laboratory of Medical Microbiology and Virology, IRCCS San Raffaele Scientific Institute; via Olgettina 60, 20132 Milan, Italy
9. Department of Experimental Oncology, European Institute of Oncology IRCCS, 20139 Milano, Italy.
10. Department of Oncology and Hematology-Oncology, University of Milan, Via Festa del Perdono 7, 20122 Milano, Italy
11. Department of Biology and Biotechnologies, University Sapienza Rome, Via Aldo Moro 5, 00185, Roma, Italy

[#]These authors equally contributed

[$]Correspondence to: roberto.giambruno@itb.cnr.it; gian.tartaglia@iit.it; francesco.nicassio@iit.it;

Abstract

SARS-CoV-2 is a positive single-stranded RNA virus that interacts with proteins of infected cells at different stages of its life cycle. These interactions are necessary for the host to recognize and block the replication of the virus. Yet, if cells fail to block SARS-CoV-2, host proteins are recruited to translate, transcribe and replicate the genetic material of the virus. To identify the host proteins that bind to SARS-CoV-2 RNA, we adopted the RNA-Protein Interaction Detection coupled to Mass Spectrometry (RaPID-MS) technology, which allows the purification and identification by MS-based proteomics of the proteins associated with a specific RNA of interest expressed in mammalian cells. We specifically investigated proteins associated with the 5′ and 3′ end regions of SARS-CoV-2 RNA. As associations might involve non-physical protein-RNA interactions, we defined a set of reliable protein-RNA interactions by exploiting the predictive power of the *cat*RAPID algorithm that assesses the direct binding potential of proteins to a given RNA region. Among these specific SARS-CoV-2 RNA end interactors, we identified the pseudouridine synthase PUS7 that binds to both 5′ and 3′ ends of viral RNA, which harbor the canonical consensus sequence modified by PUS7. We corroborated our results through SARS-CoV-2 RNA analysis by nanopore direct RNA sequencing. Indeed, these PUS7 consensus regions were found highly modified on viral RNAs, as demonstrated by ionic current features that are significantly different compared to the unmodified *in vitro* transcribed RNA. Overall, our data map the specific host protein interactions of SARS-CoV-2 RNA and point to a role for cellular pseudouridine synthases and the post-transcriptional pseudouridine modifications in the viral life cycle.

Introduction

The outbreak of severe acute respiratory syndrome coronavirus 2 (SARS-CoV-2) in the human population has dramatically affected life expectancy worldwide. SARS-CoV-2 infection causes the coronavirus disease 2019 (COVID-19), a potentially fatal condition especially for the elderly population and for individuals with underlying health issues. To date, vaccination is the most effective strategy to significantly reduce the incidence of SARS-CoV-2 infection and the onset of severe COVID-19. However, new and fast-spreading SARS-CoV-2 variants might be able to escape from the antibody response of vaccinated people (1).

SARS-CoV-2 is a positive-sense single-stranded RNA virus of the Coronoviridae family (2, 3). Its genome is composed of ~30.000 nucleotides and contains 14 open reading frames (ORFs) encoding 16 non-structural proteins (nsp 1 to 16), 12 accessory proteins (ORF3a, ORF3b, ORF3c, ORF3d, ORF6, ORF7a, ORF7b, ORF8, ORF9b, ORF9c, ORF9d and ORF10) and 4 structural proteins: spike (S), envelope (E), membrane (M) and nucleocapside (N) (4–6). Structural and accessory proteins are encoded in subgenomic RNAs (sgRNAs) that bear a common 5′ leader sequence fused to different body sequences upstream to the encoded ORF (7). During its life cycle, SARS-CoV-2 RNAs interact with several host proteins specifically required for the translation of viral proteins, the transcription of the subgenomic RNAs, the replication of the genome and the generation of new viral particles (8). At the same time, proteins of the host recognize the presence of the SARS-CoV-2 RNA in the cytoplasm, activating the innate immune response through the interferon signaling pathways (9–11). Although the interaction between viral RNAs and host proteins has been recognized as a key molecular process for virulence, we have not yet achieved a complete and clear understanding of these interactions and their underlying mechanisms.

Several laboratories have independently mapped the SARS-CoV-2 RNA–host protein interactome in mammalian cell lines that are permissive to SARS-CoV-2 infection (12–15). In these studies, the interactome was analyzed using an RNA-centric approach to specifically purify the viral RNA at 8h-24h post-infection, a time frame in which the virus is actively replicating and produces viral proteins that hijack the host innate immune response (16, 17). Many host RNA-binding proteins (RBPs) have been reported to interact with the SARS-CoV-2 RNA. These RBPs are involved in different biological processes such as RNA splicing, RNA metabolism, nonsense-mediated decay, translation and viral processes. However, the

interactions between host proteins and viral RNAs at earlier stages of the viral life cycle remain largely undetected. As well as, the assessment of the RNA regions that are specifically bound by the host proteins. With this work, we aim to fill these gaps by expressing defined SARS-CoV-2 RNA fragments in human living cells and analyzing the interaction with the host proteins that might occur in the absence of viral proteins. In particular, we focused on the highly structured regions containing the 5′ and the 3′ ends of SARS-CoV-2, which we previously predicted to be interaction hot spots for the host proteins, as observed also for other coronaviruses (18).

To thoroughly investigate the interactome of these key regions of SARS-CoV-2 RNA, we used a rational approach based on the combination of the *in house* algorithm *cat*RAPID and the well established RNA–Protein Interaction Detection-Mass Spectrometry (RaPID-MS) approach (19). We retrieved several host proteins that interact with SARS-CoV-2 genomic RNA, some already reported and other unveiled RBPs which may have key functions in the early phases of viral infection. In particular, we discovered the interaction with pseudouridine synthase 7 (PUS7) enzyme, an RNA modifier which catalyzes the pseudouridylation of RNA transcripts. Nanopore direct RNA sequencing of SARS-CoV-2 RNA from infected mammalian cells confirmed the link between pseudouridylation and viral RNAs. We found that SARS-CoV-2 subgenomic RNAs carry several post-transcriptionally modified uridines and some of them are present within the PUS7 consensus sequence. Hence, our study suggests that the activity of cellular pseudouridine synthases could strongly influence SARS-CoV-2 life cycle.

Results

Prediction of SARS-CoV-2 regions with the highest propensity to interact with host proteins

Our recent analysis of the SARS-CoV-2 RNA identified the first and last 1.5 kilobase (kb) of the viral genome as the most structured regions (18). Previously, we demonstrated that RNA regions with high structural content tend to tightly interact with a large number of proteins (20, 21), which indicates that structured regions of SARS-CoV-2 RNA genome might play a crucial role in its life cycle (22). In line with this observation, other works have reported that the first and last 1.5 kb of the viral genome recruit specific factors required for viral translation and replication, and that they act as targets for the intracellular host defense response (23, 24). To accurately map the regions with the highest propensity to interact with host proteins, we computationally fragmented the initial and terminal 1.5 kb regions of the viral genome into 500 nucleotide-long RNA fragments. Each fragment overlaps the following one by 250 nucleotides. We obtained a total of five fragments for the 5′ region (numbered 1 to 5) and five for the 3′ region (numbered 6 to 10) (**Supplementary Table 1** and **Fig. 1A**). We then employed the *cat*RAPID algorithm (25), which estimates the binding affinity of protein-RNA interactions (26, 27), to predict the interactions of each fragment with human RNA-binding proteins (RBPs, over 2000 entries; **Supplementary Table 2**). We identified fragments 1 and 2 and fragments 9 and 10 as those having the strongest scores (**Fig. 1B**). Considering that the 5′ and 3′ UTRs (fragments 1 and 10) have the strongest scores, we reasoned that these regions might also be the most functionally relevant (28). Altogether, these results provide important indications on the location of structural hot spots potentially relevant for the functional interactions between the virus and the host.

Identification of the human interactome for the 5′ and 3′ ends of SARS-CoV-2 genome

We exploited the RaPID-MS approach using the 10 above described fragments analysed with *cat*RAPID (**Fig. 1A**) (29). The fragments were cloned within BoxB-sequences (**Materials and Methods**), used as tags for the RaPID assay, and were expressed into HEK293T cells as host cell line (**Fig. 1C**). All RNA fragments were predicted to fold according to the secondary structure presented in **Supplementary Fig. 1**. As a negative control, we generated a scrambled sequence of 500 nt of similar GC content compared to the other fragments (named ‘Scramble’ henceforth). The BoxB-tagged EDEN15 RNA was selected as positive control (19). We

controlled that: i) each plasmid expressing an RNA fragment was co-expressed with a plasmid coding for the λN-HA-BASU biotinylating enzyme by FACS analysis (**Supplementary Fig. 2)**; ii) the correct expression of λN-HA-BASU and the biotinylation of the protein substrates in the presence of exogenous biotin by Western Blot (WB) analysis (**Supplementary Fig. 3A**). The resulting biotinylated proteins were purified using streptavidin beads under denaturing conditions, as confirmed by WB analysis (**Supplementary Fig. 3B**) and analyzed by liquid chromatography tandem mass spectrometry (LC-MS/MS). In total, 3 independent biological replicates of RaPID-MS were performed using the 10 SARS-CoV-2 fragments, as well as the Scramble and the EDEN15 RNAs. The retrieved proteins are reported in **Supplementary Table 3.** We identified a total of 1296 proteins interacting with our selected fragments. A comparison between our dataset and the ones generated by previous studies indicates an overlap of >37% (**Supplementary Table 3)**, demonstrating a good agreement with the literature (22, 30). We were interested in finding host proteins that specifically bind to SARS-CoV-2 RNA fragments rather than promiscuously any RNA. Therefore, we compared the list of interactors obtained with each individual fragment with those obtained with our negative control Scramble (**Supplementary Fig. 4A and 4B and Supplementary Table 3**). Our approach correctly worked, since we identified CELF1 as a specific interactor exclusively of our positive control EDEN15 (**Supplementary Fig. 4B**), as previously reported (31). The proteins associated with the SARS-CoV-2 RNA fragments to the same extent of our negative and positive controls were removed from the final list of specific interactors, including RBPs such as PTBP1, G3BP1 and SYNCRIP that were previously reported to specifically interact with the SARS-CoV-2 RNA (12–15) (**Supplementary Table 3)**. In total, we identified 73 proteins significantly interacting with SARS-CoV-2 RNA fragments, hereafter called RaPID-MS dataset (**Figure 2**). Of the RaPID-MS dataset, 10 proteins were previously reported as interactors of SARS-CoV-2 RNA, namely FAM120A, HAT1, LSG1, SHMT1, SYNE2 and the ribosomal proteins RPL14, RPL18A, RPL24, RPL35, RPS6; while the remaining 63 were identified for the first time (**Supplementary Fig. 5a and 5b)**. The highest number of interacting proteins were in fragments 1, 4, 7 and 10. Conversely, fragment 2 displayed only two specific interactions (**Fig. 2A**). The median enrichment value of each significant interactor was corrected for protein length and abundance to eventually balance the bias that could be introduced by the RaPID technique (**Fig. 2B**). As for other studies of SARS-CoV-2 RNA interactome (32), we retrieved ribosomal proteins (N=7) among the most highly enriched interactors (**Fig. 2B**), explained by the fact that some of the fragments contain open reading frames (ORFs). We expected the RaPID-MS dataset to be enriched for direct RNA-protein

interactions. Indeed, 73% (53/73) interactors are annotated as RBPs according to the RBPome database (https://rbpbase.shiny.embl.de/) (green circles in **Fig. 2C**). While some proteins (N=26) were shared among 2 or more fragments, most interactions (N=47) were specific for just one RNA fragment (**Fig. 2C)**. In some cases, the proteins most likely interact with the overlapping regions included within the fragments. Examples are the proteins WNK3 and AP4M1, which were found in association with the neighboring fragments 4 and 5 and fragments 7 and 8, respectively. Interestingly, three proteins (CEP350, RGPD1 and GPKOW) were exclusively interacting with the two terminal fragments (1 and 10), suggesting they might bind 5′ and 3′ ends independently or participate in viral RNA circularization, as recently described (33). Gene set enrichment analysis (GSEA) for gene ontology (GO) processes highlighted that the retrieved interactors belonged to cellular pathways involved in viral transcription, nonsense mediated mRNA decay (NMD), rRNA processing, translational initiation, mRNA splicing and mRNA export from the nucleus (**Supplementary Fig. 5c)**.

Correlation between computationally predicted and experimentally validated RNA-host protein interactors

We exploited the predicting power of the *cat*RAPID algorithm to select cases for further characterization (25). To properly compare predicted and experimental interactions, the median enrichment value of each experimentally identified interactor was normalized by protein length and abundance (**Supplementary Table 4**). We restricted the computational prediction analysis to human RBPs reported in the *cat*RAPID library (25), here named RaPID-RBP (**Supplementary Table 4**), and assessed to what extent the predicted binding propensities are in agreement with the experimental results obtained in the RAPID-MS dataset. In particular, we verified whether the strongest positive (i.e. interacting) and strongest negative (i.e. non-interacting) predicted protein-RNA pairs could be identified in the list of experimentally validated interactions. We evaluated the performance of our prediction using the Area Under the ROC Curve (AUC). Overall, *cat*RAPID reached an AUC of over 0.80. The AUC increased from 0.58 to 0.83 when applying the predictions to the experimental scores from the top 20% (i.e. the 20% strongest positives vs the 20% strongest negatives) to the top 2.5% (i.e. the 2.5% strongest positives vs the 2.5% strongest negatives) (**Fig. 3A** and **Supplementary Table 4**). When considering each fragment separately, the prediction performances increased even further for the terminal regions of the viral genome (fragments 1 and 10) and for some internal

overlapping fragments (4, 5, 6), reaching an AUC of 0.95 for the top 1% ranked experimental cases (**Fig. 3B and Supplementary Table 4**). Overall, this analysis suggests that predicted and the experimental data are well correlated.

Prompted by this observation, we exploited the *cat*RAPID score to produce a rank of the RBP interactome of SARS-CoV-2 RNA identified by RAPID-MS. The $\log_2$ *cat*RAPID score for all the possible viral RNA-host protein interactions was between 3.22 and 6.70, with a median value of 4.62 (**Fig. 3C and Supplementary Table 4**). The *cat*RAPID predicted RNA-protein interactions of each viral RNA fragment were differently distributed within these intervals (**Supplementary Figure 6A-B**). In particular, proteins above a $\log_2$ *cat*RAPID score of 5.22, corresponding to the 85th percentile and the graphical inflection point of the distribution, are significantly enriched for interactions with Fragment 10, 4 and 5 (**Fig. 3C and Supplementary Table 4**). These three fragments together displayed 373 predicted interactions that were not found with the RNA control Scramble, including 13 interactions that involved 9 RBPs significantly associated with the SARS-CoV-2 RNA fragments by RaPID-MS (**Fig. 3D**). Among them, i) FAM120A, LSG1 and RPS6 that were already reported as host proteins reproducibly interacting with SARS-CoV-2 RNA (32); ii) the splicing factors GPKOW, SF3A1, NOP58 and the NDM factor SMG7 that were computationally predicted to specifically associate to the genomic viral RNA (34, 35); iii) the RNA modifier PUS7, that catalyzes the isomerisation of uridine into pseudouridine in cellular tRNAs and mRNAs, reported here for the first time. In the RaPID-MS dataset, PUS7 specifically associates with fragments 1, 4, 7 and 10, all harboring a PUS7 consensus sequence. In agreement with our finding, pseudouridine has been found as the most abundant modification in SARS-CoV-2 RNA (10) and another member of the pseudouridine synthase family, PUS1, has been reported to interact with SARS-CoV-2 RNA (14). These observations strongly suggest that, in human cells, the formation of pseudouridine residues on SARS-CoV-2 genome could be catalyzed by the activity of cellular RNA-independent pseudouridine synthases, such as PUS1 and PUS7.

SARS-CoV-2 subgenomic RNAs bear multiple putative pseudouridylated sites

To investigate occurrence of pseudouridine sites in SARS-CoV-2, we employed Nanopore direct RNA sequencing (DRS) on cell lines infected with SARS-CoV-2 and analyzed the data with the Nanocompore software package (**Materials and Methods**). Nanocompore searches for RNA post-transcriptional modifications by comparing the ionic current features generated

by Nanopore DRS from two different experimental conditions: a test sample and a reference, which is devoid of the modification of interest (or with a reduced number of them) (36). We focused on all the 14 canonical viral subgenomic RNAs (sgRNAs) of SARS-CoV-2 (Figure 4A and Supplementary Table 5, 6, 7) used by the virus to translate the structural and accessory proteins required to produce new virions and that we recently characterized by employing Nanopore ReCappable Sequencing NRCeq, a new technique that can identify capped full-lenght RNAs (6). In this instance, we compared viral sgRNA from infected Vero E6, CaCo-2 and CaLu-3 cells to an unmodified SARS-CoV-2 RNA obtained by *in vitro* transcription (IVT) (37). Sequenced reads were aligned to the most up-to-date viral reference transcriptome (6) and the ionic current features from the RNA reads were realigned to each transcriptomic position of the reference using Nanopolish (38). Then, we used Nanocompore to identify RNA post-transcriptional modifications as marked by differences in the electrical signal between the viral sgRNA reads and the IVT RNA reads. Due to the physics of nanopore sequencing, Nanocompore compares the ionic current features of five nucleotides (named as k-mer) at a time. To identify putative pseudouridine sites, we filtered the results by selecting k-mers that contained at least one uridine and identified as significant by Nanocompore (p-value ≤ 0.01, absolute value of the log odds ratio (LOR) ≥ 0.5). Using these filtering conditions, we identified 1165 (CaCo-2), 430 (CaLu-3) and 628 (Vero E6) significant uridine-containing k-mers, distributed among the 14 canonical SARS-CoV-2 reference sgRNAs (**Figure 4A, Supplementary Figure 7** and **Tables 5-7**).

To focus on sites consistently modified across samples, we considered significant modified RNA nucleotides that were identified in at least two out of three SARS-CoV-2 infected cell lines (see **Materials and Methods**). Overall, we obtained 457 candidate modified regions across the 10 different SARS-CoV-2 sgRNAs encoding for canonical ORFs (**Figure 4B)**. Importantly, two of these regions were recently described as a pseudouridine site in SARS-CoV-2 genomic RNA (39) (**Supplementary Table 9**).

To shortlist from the 457 sites that we identified the ones with a higher likelihood of being PUS7 targets, we selected those overlapping the RNA consensus sequence of PUS7. We found that 53 sites had the more generic PUS7 consensus sequence UNUAR (red lollipops of **Figure 4B)**, while eight had the more restrictive UGUAR motif (red lollipops with displayed sequence of **Figure 4B)**. Interestingly, six sites are located within RaPID fragments 1 and 10, which were bound by PUS7 in our interactomic data (**Supplementary Table 8** and **Figure 2C**). The modified sites containing the UGUAR consensus were manually inspected to confirm that the

distributions of ionic current intensities and dwell times were different between the IVT and SARS-CoV-2 reads in a window of nine k-mers centered on the central U of the UGUAR motif (**Supplementary Figure 8)**. Interestingly, we observed that three of these sites were present within the Transcription Regulatory Sequence (TRS-L) at the 5′ UTR of the sgRNAs encoding for ORF10, NS6, and VME1 (**Figure 4B** and **Supplementary Table 9**), suggesting that the deposition of pseudouridine within the TRS-L might contribute to the regulation of sgRNA production or viral protein synthesis.

Discussion

The identification of host proteins interacting with SARS-CoV-2 RNA is of fundamental importance for the development of molecules that block virus replication in human cells. Host proteins transiently interact both with the SARS-CoV-2 genomic and subgenomic RNAs to contribute to the different steps of the viral life cycle including translation, transcription and replication. Four independent studies have characterized the host and viral protein interactome of SARS-CoV-2 RNA genome in human cells at different time points, providing a global picture of the interactions occurring in infected cells. However, there is a relatively poor overlap between the interactors retrieved in these studies (22, 30), most likely attributable to the different permissive host cells used, the time of infection of the assay and the strength of interactions and the type of crosslinking agents adopted to enrich for RNA-protein interactions (32). Moreover, in infected cells, host proteins can concurrently interact with the viral genomic RNA, subgenomic viral RNAs or both.

To unveil the SARS-CoV-2 RNA-host protein interactions occurring at the initial stages of viral infection in human cells, we decided to exploit the proximity ligation technology RaPID-MS (19), specifically focusing on the most predicted structured regions of SARS-CoV-2 RNA. Even though our analysis was performed in non-infected cells, we identified the proteins FAM120A, HAT1, LSG1, RPL14, RPL18A, RPL24, RPL35, RPS6 SHMT1 and SYNE2 that were also obtained by the other studies performed in SARS-CoV-2 infected cells, confirming the reliability of our approach. Compared to other approaches, our strategy has two main advantages: i) it does not involve any crosslinking step, minimizing the number of proteins indirectly associated with SARS-CoV-2 RNA; ii) it detects viral RNA-host protein interactions that occur during the early phase of infection, when viral proteins are poorly expressed and the virus is strictly dependent on the host proteins. For instance, among the retrieved SARS-CoV-2 RNA fragment-host protein interactions, we found three proteins CEP350, GPKOW and RGPD1 that are exclusively interacting with the fragments containing the 5′ and 3′ UTR regions. These proteins may be required for the genome cyclization process that possibly regulates SARS-CoV-2 RNA discontinuous transcription, as recently reported (5, 33).

The fact that numerous RBPs were identified as non-specific RNA binders suggests that several interactions participate in host mechanisms triggered by the accumulation of viral RNAs in infected cells. The accumulation of viral RNA - host RBP interactions is likely caused by the formation of stress granules (SGs) that are required for the sequestration of viral RNA by the

host to suppress viral replication (30). Indeed, several of the RBPs defined by us as promiscuous binders are involved in SGs formation and composition, such as the SG nucleating factors G3BP1 and G3BP2 and the proteins CAPRIN1, PUM1 and PUM2, respectively (40).

SARS-CoV-2 RNA is heavily post-transcriptionally modified (41), although the role of every RNA modification has not been fully described. In particular, m6A is known to be deposited by METTL3 on SARS-CoV-2 RNA and impair the binding of the viral RNA sensor RIG-I, thus bypassing the innate cellular immunity response (10, 42). Similarly, pseudouridine, which is documented to be the most abundant modification identified in SARS-CoV-2 RNA, has been hypothesized to aid the virus to hijack the host immune sensors and evade the innate immune response (10). The writer enzyme responsible for this modification is still unknown, although PUS1, a member of the pseudouridine synthase family, was found to be associated with SARS-CoV-2 RNA (14). In our RaPID-MS analysis we found that another member of the pseudouridine synthase family, PUS7, binds to the RNA fragments present at both the 5′ and 3′ end regions of the viral genome. The interacting RNA fragments carry the PUS7 consensus sequence UGUAR, corroborating the evidence that PUS7 might be one of the enzymes responsible for the pseudouridylation of SARS-CoV-2 RNA. In agreement, our DRS analysis on mammalian cells infected with SARS-CoV-2 revealed the presence of 53 sites containing PUS7 consensus sequences that display a significant difference in electrical signal distribution compared to the unmodified *in vitro* transcribed RNA. These data suggest that PUS7 is specifically recruited to its UGUAR consensus sequences in the 5' and 3' ends of the viral RNA, where it can catalyze the formation of pseudouridine, with potential regulatory effects on the RNA secondary structure or its interaction with host-proteins.

Interestingly, three of the UGUAR sites identified by Nanocompore overlapped with a region of the TRS-L within stem loops 2 and 3 of the SARS-CoV-2 5′ UTR. This region has been demonstrated to fine-tune RNA ribosomal loading through the modulation of its structural domains (43). Pseudouridylation dependent TRS-L conformational change is potentially a mechanism for regulating sgRNA translation. Although this is likely a mechanism for all sgRNAs, we only detected the putative pseudouridine sites in three of the ten canonical SARS-CoV-2 ORF-grouped sgRNAs. This is likely due to the 3′ end coverage bias of DRS reads (44) and the minimum k-mer coverage requirements of Nanocompore. It is possible that this modified site would have been identified in all the sgRNAs if we had improved the 5′ end coverage.

The combination of the interactomic analyses and RNA modification profiling of SARS-CoV-2 RNA proposes a putative role for pseudouridine in SARS-CoV-2 biology that will require further experimental validation. Additional investigation is needed to determine whether other pseudouridine synthases can modify SARS-CoV-2 RNA, even within the PUS7 consensus sequence. In particular, PUS1 has been recently described to be able to modify UGUAG-containing RNA sequences (45). Considering the high viral copy numbers present in cells where SARS-CoV-2 is actively replicating, it is reasonable to imagine that several pseudouridine synthases might act on the viral RNAs at the same time. Thus, a comprehensive understanding of the molecular mechanism regulating the pseudouridylation of SARS-CoV-2 RNA could be crucial for the development of alternative strategies to impair viral replication in infected human cells.

Materials and methods

Preliminary predictions of protein-RNA interactions

The c*at*RAPID algorithm (25, 46) was used to identify the binding propensity of the 10 SARS-CoV-2 500 bp fragments against a library of 2064 human RBPs. For each fragment, only the interactions with associated propensity score > 85th percentile of the fragment score distribution were retained and subsequently, the average score was calculated.

Reagents and plasmids

The following plasmids were purchased from Addgene and used for the RaPID-MS assay: BoxB-plasmid (Addgene #107253); BoxB-EDEN15 plasmid (#107252); BASU RaPID plasmid (#107250).

All the plasmids were a gift from Paul Khavari (Addgene plasmid #107253; #107252; #107250. http://n2t.net/addgene: 50917; 107252; 107250. RRID : Addgene_50917; Addgene 107252; Addgene 107250) (Ramanathan et al., 2018). SARS-CoV-2 RNA fragments, derived from the SARS-CoV-2 RNA sequence MN908947.3, were synthesized by GeneArt (ThermoFisher Scientific) according to the sequence reported in **Supplementary Table S1**, flanked by Esp3I restriction sites. The same strategy was adopted for the Scramble control sequence: 3′-CGTCTCCGCTTTCGACGACAATTTATAAAGACAGCGGTCGAGGGAAGATTTACGAGTTGAATCGAGATGCGCTGATTCGACGCAGTGTCGCGTTGTGGTGAGGTAAATTGATAGGTGTATTTTGCGAGATACAGTGATGAACACTTCATTAACAACATGATTTATACGACGATTACTAGAATTATGAAAAATGAGTCATCTACAAGCGCGTTTTTACATTGCCGTGGTTAATCGTAAGGATAGCACAGTTAACAGCGGACCCCGGCGGACTCGGCCCTATCTGAACGAATTGAGCTCCGTTCGAAATATCTAGTGAATGACCCTCCCCACGTGCCTTGATAAGCCGTGGTATTTCGTATCATACAAGTTCCAGAAGGATGGTTCAACATAGTAGGGTACCGACTGGATAGAACAAACTACTCATGTTTTCGCCGGGGGACGAACGGTAAGCTCCGCTGGGTTGACTTCTTGACCAAAGTATTTGGGTATCCAAACAGTGCCGTTAACAGCCAAGCTAGAGACG-5′.

The RNA fragments were then cloned into the pLEX BoxB-plasmid using the Esp3I sites, as described in literature (29).

The following antibodies were used in this study**:** Streptavidin-HRP (Cat. #3999) from Cell Signaling Technology. Anti-Vinculin (Clone H Vin 1 0,2 Ml; Cat. #V9131) from Merck. Anti-HA-11 epitope tag, clone 16B12 from Biolegend (Cat #901501).

Cell lines

HEK293T cells were grown in DMEM with Glucose and L-Glutamine (Lonza, BE-12-604Q) supplemented with 10% fetal bovine serum (FBS) Tetracycline free (Euroclone, ECS01822) and 100 U/ml Penicillin and Streptomycin. CaCo-2 cell lines were cultivated in Minimum Essential Medium Eagle (MEM) (Merck, M4655) complemented with 20 % FBS Tetracycline free, 2 mM L-Glutamine (Lonza, BE17605E), 1 mM Sodium Pyruvate (Lonza, BE13115E), 0.1 mM not essential amino acids (Lonza, BE13114E) and 100 U/ml Penicillin and Streptomycin (Euroclone, ECB3001D).

Virus isolation and cell infection

SARS-CoV-2 virus was isolated from a mildly symptomatic SARS-CoV-2 infected patient, as described in Ugolini et al. (6). CaCo-2 cells were infected at 80% confluency into a 25 cm2 tissue culture flask with SARS-CoV-2 at 0.1 Multiplicity of infection (MOI). After 1 h adsorption at 37°C, cells were washed with PBS, and further cultured at 37°C for 48 h with 4% FBS. After a PBS wash, enzymatic dissociation was performed for 4–6 min at 37°C in 1 ml TrypLE (Invitrogen), then cell pellets were washed with ice-cold PBS and lysed with 1 ml of TRIzol (Invitrogen). The samples were stored at −80°C for subsequent RNA extraction.

RNA extraction and nanopore direct RNA sequencing

RNA was extracted from CaCo-2 cells infected with SARS-CoV-2 using the RNeasy Mini kit (Qiagen) including an in-column DnaseI treatment step, following the manufacturer protocol. The isolated RNA was then processed by direct RNA sequencing protocol as described in Ugolini et al. (6).

RaPID assay

The RaPID protocol was performed as reported (29) and slightly adapted as described below. HEK293T cells were transfected with plasmid vectors expressing λN-HA-BASU and one of the BoxB-RNA fragments using Lipofectamine™ 3000 transfection reagent (L3000001;

ThermoFisher Scientific), according to vendor's instructions. After 48h from transfection, medium was changed and replaced with standard growth medium complemented with 200 µM biotin (Merck, B4639-1G) for 1 hour. Cells were harvested, washed once with PBS 1x and lysed with RIPA buffer (10mM Tris-HCl pH 8.0, 1%Triton-X100, 150mM NaCl, 0.1% SDS, 0.1% NaDeoxycholate, 1mM EDTA) supplemented with 1mM 1,4-Dithiothreitol (DTT), cOmplete™ Protease Inhibitor Cocktail (11697498001; Merck) and PhosSTOP™ (4906845001; Merck). Cell lysates were incubated for 15 minutes on ice and then centrifuged at 15000 g for 15 minutes. The supernatants containing the protein extracts were transferred into fresh 1.5 ml tubes and protein concentration was measured by Bio-Rad Protein Assay Kit using BSA as protein standard (5000002; Bio-Rad). From each sample, 3 mg of protein extract was taken and brought to the same volume (600uL) with RIPA buffer. 5% of input material was taken for further analysis and 150 uL of pre-washed Streptavidin Mag Sepharose® (GE28-9857-99; Merck) were added to the remaining material. Then, samples were rocked over night at 4C. The following day, beads were separated from the unbound fractions and 5% of each fraction was collected in fresh tubes. Beads containing the biotinylated proteins were washed 3 times with 1 mL of Wash Buffer 1 (1% SDS supplemented with 1mM DTT, protease and phosphatase cocktail inhibitors); 1 time with Wash Buffer 2 (0.1% Na-DOC, 1% Triton X-100, 0.5M NaCl, 50mM HEPES pH 7.5, 1µM EDTA supplemented with 1mM DTT, protease and phosphatase cocktail inhibitors) and 1 time with Wash Buffer 3 (0.5% Na-DOC, 150mM NaCl, 0.5% NP-40, 10mM Tris-HCl, 1µM EDTA supplemented with 1mM DTT, protease and phosphatase cocktail inhibitors). All the washes were performed by rocking samples for 5 minutes at 4 °C. Finally, proteins were eluted with Laemmli buffer containing 100 mM DTT and boiled for 5 minutes at 95 °C.

In-gel digestion

Eluted biotinylated proteins were processed as previously described by (47). Briefly, proteins were initially separated on a precast 4-12% gradient gel (NP0322BOX, ThermoFisher Scientific). Each lane was divided in 6 slices that were cut from gels and destained in 50% v/v acetonitrile (ACN)/50 mM NH_4HCO_3. A reduction step was performed with 10 mM DTT, followed by alkylation with 55 mM iodoacetamide in the dark. After each step, samples were dehydrated with 100% ethanol and quickly dried in a centrifugal evaporator (SpeedVac). Subsequently, gel pieces were washed with 50 mM NH_4HCO_3 and overnight digested with 12.5 ng/ml trypsin (Promega, V5113) at 37 °C. The following day, tryptic digested peptides

were extracted with Extraction Buffer (3% TFA, 30% ACN) and 100% ACN. Prior to MS, peptides were desalted and concentrated in a single step through reversed phase chromatography on micro-column C18 Stage Tips (Rappsilber et al., 2007) and eluted in 0.1% formic acid (FA).

Nano-LC-MS/MS analysis

Peptide mixtures were analyzed by online nano-flow liquid chromatography tandem mass spectrometry using an EASY-nLC 1000 (Thermo Fisher Scientific, Odense, Denmark) connected to a Q-Exactive Plus instrument (Thermo Fisher Scientific) through a nano-electrospray ion source. The nano-LC system was operated in one column set-up with a 50-cm analytical column (75 µm inner diameter, 350 µm outer diameter) packed with C18 resin (EasySpray PEPMAP RSLC C18 2 µm 50 cm x 75 µm, Thermo Fisher Scientific) configuration. Solvent A was 0.1% FA in water and solvent B was 0.1% FA in 80% ACN. Samples were injected in an aqueous 0.1% TFA solution at a flow rate of 500 nL/min and separated with a gradient of 5%–40% solvent B over 50 min followed by a gradient of 40%–60% for 10 min and 60%–80% over 5 min at a flow rate of 250 nL/min in the EASY-nLC 1000 system. The Q-Exactive was operated in the data-dependent mode (DDA) to automatically switch between full scan MS and MSMS acquisition. Survey full scan MS spectra (from m/z 300-1150) were analyzed in the Orbitrap detector with resolution R = 35,000 at m/z 400. The ten most intense peptide ions with charge states R 2 were sequentially isolated to a target value of 3e6 and fragmented by Higher Energy Collision Dissociation (HCD) with a normalized collision energy setting of 25%. The maximum allowed ion accumulation times were 20 ms for full scans and 50 ms for MSMS and the target value for MSMS was set to 1e6. The dynamic exclusion time was set to 20 s.

Data analysis of MS data

Proteins were identified and quantified using MaxQuant software v.1.6.0.16. using the Andromeda search engine (48, 49). In MaxQuant, the false discovery rate (FDR) of all peptide identifications was set to a maximum of 1%. The main search was performed with a mass tolerance of 6 ppm. Enzyme specificity was set to Trypsin/P. A maximum of 3 missed cleavages was permitted and the minimum peptide length was fixed at 7 amino acids. Carbamidomethylation of cysteines was set as a fixed modification. The 2021_01 version of the human UniProt reference proteome (UP000005640) was used for peptide identification.

Proteins were profiled by quantitative label-free analysis, activating the label-free software MaxLFQ (48) and analyzed using Perseus software (50), plotting the LFQ values in a volcano plot graph, where the proteins enriched with each SARS-CoV-2 RNA fragments were compared to the Scramble RNA control. The p-Value was calculated by Perseus using a two-tailed *t*-Test. Missing values were replaced by the minimum detection value of the matrix. Proteins found as significantly enriched also with the EDEN15 RNA were removed from the final network. The interaction network generated with the statistically significant proteins was visualized using Cytoscape 3.8.1 (51).

RNA folding analysis

Predictions of RNA folding were performed using the RNAfold algorithm hosted in ViennaRNA Web Services (52) using the default parameters and displaying the centroid secondary structures.

Gene Ontology (GO) Analysis

The GO analysis was performed on the 73 proteins specifically associated with the 10 SARS-CoV-2 RNA fragments and identified by RaPID-MS using the GOTERM biological process (BP) and molecular function (MF) present in the DAVID 6.8 Bioinformatics Resources (https://david-d.ncifcrf.gov/home.jsp) (53)

Computational evaluation of experimental interactions

The *cat*RAPID algorithm was used to assess the predictive accuracy on the experimental RAPID dataset. Here, for each SARS-CoV-2 fragment-human protein pair, a fragmentation procedure was performed to identify the binding regions. The propensity score is calculated taking into consideration the maximum and the minimum score of all the sub-fragments computed by the algorithm (25) and computing their difference (54) . The median LFQ value for each protein-fragment pair was then normalized taking into account protein abundance in HEK293 cell lines from PAXdb (55) and protein length from UniProt database (56), using the following equation:

Normalized LFQ value = LFQ – 0.6*log2(abundance)-0.0001*log2(length).

This approach was introduced to reduce the experimental bias in LFQ scores with high protein abundance and length.

Nanopore DRS and Nanocompore analysis

The nine DRS datasets were compared to the IVT dataset, using the NRCeq assembly and the methods in (6). The dataset of Vero E6 cells, Calu-3 and CaCo-2 sample 1 and 2 are derived from (6) (ENA ID: PRJEB48830); CaCo-2 sample 3 and 4 are deposited with this manuscript (ENA ID: PRJEB53497). Reads were grouped by cell type and their fastq files concatenated. Reads were resquiggled using F5C (v0.6) (57) (**Suppl. Table 5, 6, 7**). IVT reads were separately mapped to each reference sgRNA using minimap2 (v2.17-r974-dirty) (58) with the following parameters: -ax map-ont -p 0 -N 10.

Nanocompore (v1.0.4) (36) was used to detect RNA modifications by comparing the IVT reads to a set of reads from each cell line for every reference sgRNA with the subsequent parameters:

--fasta <NRCeq_assembly_fasta_file> --overwrite --downsample_high_coverage 5000 --allow_warnings --pvalue_thr 0.01 --min_coverage 30 --logit --nthreads 3 --bed <NRCeq_assembly_bed_file> .

Cell line - specific analysis

The following analysis was performed on Nanocompore output for each cell line. K-mers were considered significant if they had a GMM_logit_p-Value ≤ 0.01, an absolute value of LOR ≥ 0.5, and one of the 5 nucleotides was a uridine. Significant k-mers were removed if they were within 15 nt of a TRS-L/B junctions (ORF junctions) or 25 nt of an IVT fragment boundary (IVT junctions) (37), because these regions are prone to aberrant signal artifacts that can cause false positives.

A single modification can affect multiple k-mers, thus we used the find_peaks function from scipy.signal (59) to merge neighboring significant sites into unified peaks. The -log10 (p-values) of U-containing k-mers were used for peak calling with a threshold of 2 and a width of 5. Any of these k-mers that were within 15 nt of an TRS-L/TRS-B junction or 25 nt of an IVT junction were also removed as described above. Only k-mers which aligned to reference sgRNAs with the TRS-L/B junction next to ORF9d, ORF10 and canonical reference sgRNAs

were included because early-terminating non-canonical sgRNAs were shown to be problematic to map correctly (6).

The resulting sites were compared to those identified in Fleming et al. (39) by creating an array with genomic positions of the five nucleotides for every significant k-mer. The R function "%in%" was used to compute the intersection between each of these arrays and an array containing the genomic positions of Fleming et al. "high-confidence sites" (39). Any k-mer with a nucleotide that overlapped with the "high-confidence" sites was considered a match.

Data was visualized using the UCSC Genome Browser tracks from BED files of the peakcalled and filtered k-mers (60).

Merging analysis

Individual significant k-mers from the different cell lines may be offset by one or two positions, therefore the significant k-mers were transformed into larger nucleotide ranges of nine nucleotides, that include the five nucleotides of the significant k-mer, plus the two neighboring nucleotides present at both its extremities. Any of these nine nucleotides may be a post-transcriptional modified nucleotide detected by Nanocompore. In addition, we minimized ambiguous mapping by counting significant k-mers found on any isoform of VME1 and NCAP as a single isoform according to their genomic coordinates.

Sites were compared to the high-confidence sites defined by Fleming et al. (39) using the single-nucleotide genomic position.

Sites were manually inspected by plotting the distribution of signal intensity and dwell time for each position using functions implemented in Nanocompore (36).

Comparison with RaPID fragments

Both significant k-mers and sites were compared with the RaPID fragments. Genomic coordinates were used for all comparisons with RaPID fragments (**Suppl. Table 1**). In the case of k-mers, we defined a RapID fragment match when the first nucleotide of the k-mer overlapped with any RaPID fragment, while for sites, we searched for every nucleotide of the site that could overlap any fragment. Genomic regions overlapping two fragments were identified with both fragment names. K-mers were assigned to each fragment based on the genomic position of their first nucleotide.

Data Availability

The mass spectrometry proteomics data have been deposited to the ProteomeXchange Consortium via the PRIDE (61) partner repository with the dataset identifier PXD034941".
The RNA sequencing datasets generated in this study have been deposited at the European Nucleotide Archive (ENA).

Acknowledgment

We thank Lorenzo di Tucci e Marco Rabozzi for developing an accelerated version of Nanopolish for preliminary analysis. The research leading to these results has been supported by European Research Council (RIBOMYLOME_309545 and ASTRA_855923), the H2020 projects (IASIS_727658 and INFORE_825080). E.Z. received funding from MINDED fellowship of the European Union's Horizon 2020 research and innovation program under the Marie Skłodowska-Curie grant agreement No. 754490.

Figure legends:

Figure 1. Experimental approach to investigate SARS-CoV-2 interactome.

A) Schematic representation of the SARS-CoV-2 RNA fragments selected to be studied with the RaPID-MS strategy. The scheme shows the fragments names, positions within the SARS-CoV-2 genome and degree of overlap between them. **B)** catRAPID predictions of the 10 selected RNA fragments with the catalogue of human RNA-binding proteins. Fragments belonging to the first and last 1.5Kbp of SARS-CoV-2 genome are colored in different shades of pink and green, respectively. Error bars for each fragment correspond to the average value ± the standard error (SE). The gray dashed line indicates the trend of the *cat*RAPID score in the chart. **C)** Description of the technique RaPID-MS, in which the RNA fragment of interest is expressed in cells flanked by BoxB stem loops. BoxB is specifically recognized by the co-transfected λN peptide fused to the biotin ligase BASU. Upon biotin addition to the growth medium, BASU biotinylates the host protein interactors attracted by the RNA of interest.

Figure 2. Defining SARS-CoV-2 interaction network with the human proteome.

A) Number of specific interactors identified for each SARS-CoV-2 RNA fragment (labeled with the letter "F" follow by a number). **B)** Enrichment distribution of the specific interactors for all considered fragments compared to the control "Scramble". Data are normalised for protein length and abundance, as specified in the Materials and Methods section. **C)** The network of proteins identified by RaPID-MS. Only proteins significantly enriched over the control "Scramble" are displayed. Data are derived from the analysis of 3 independent biological replicates. In pink are displayed the RNA fragments, while in green the retrieved interactors. Proteins circled in green are RNA-binding proteins, according to the RBPome database (https://rbpbase.shiny.embl.de/).

Figure 3. CatRAPID performances on the RaPID-RBP datasets

A) *Cat*RAPID performances on the RaPID-RBP dataset. The predictive power of the method is calculated for different percentages of the dataset. *Cat*RAPID performance is calculated on LFQ experimental value, normalised by taking into account the abundance of the proteins in PAXdb and protein length in Uniprot. **B)** *Cat*RAPID performances on the RaPID-RBP dataset, focusing on the single RNA fragments. For each fragment, the AUC at the different percentage of the dataset is shown. The performances are evaluated as in **A** and the fragments are ordered according to the respective genomic position. **C) Left.** Scatter chart of the analysed RBPs

ranked according to their relative log2 *cat*RAPID score. The dashed lines indicate the 85th percentile. **Right.** Boxplot representation of the whole distribution divided in the indicated percentiles. **D)** Scatter chart of the analysed RBPs ranked according to their relative log2 *cat*RAPID score, displaying only proteins present in the 85th percentile of the distribution.

Figure 4. Nanopore analysis identified significant k-mers in all the three analyzed cell lines. **A)** UCSC Genome Browser (*http://genome.ucsc.edu*) annotation of the modified k-mers containing a uridine found in SARS-CoV-2 infected CaCo-2, Calu-3 and Vero E6 cells and distributed over 14 different reference sgRNAs. From the top to the bottom, IVT and RaPID fragments, SARS-CoV-2 NRCeq assembly and RefSeq SARS-CoV-2 ORFs are present as a reference. **B)** Graphical representation of nucleotide ranges shared between at least two cell lines (red circles). Here, sites have been grouped per ORFs encoded by each reference sgRNA of the assembly and the sequence of those carrying an UGUAR motif is displayed.

Supplementary figure legends:

Supplementary Figure 1. Predicted RNA secondary structures of the selected BoxB-RNA fragments. The displayed RNAs represent the minimum free energy structures obtained using the ViennaRNA Web services.

Supplementary Figure 2. FACS analysis of cells co-transfected with the BoxB-RNA vector expressing also the GFP protein and the λN-HA-BASU vector expressing the RFP protein. The scatter plots showed the percentage of cells expressing the GFP, the RFP or both proteins. Untransfected cells (mock) or cells transfected with either λN-HA-BASU vector or BoxB-RNA vector were used as control to distinguish the GFP and RFP positive cells.

Supplementary Figure 3. A) Western Blot (WB) analysis of HEK293T whole cell extract (W.C.E.). Cells were transfected with plasmids expressing the λN-HA-BASU and one of the BoxB-RNA fragments. Biotin was administered into the medium 1h before cell harvesting. For WB analysis, 20 ug of each sample was loaded on a 4-12% pre-cast gel. The displayed data is the representative image of one of the three biological experiments performed. **B)** Streptavidin pulldown followed by WB analysis of the samples described in **A)**. For all samples, 3% of the eluted material (E) was loaded on a 4-12% pre-cast gel and stained with HRP-conjugated streptavidin (STREP-HRP). To control the efficiency of the streptavidin pulldown, 5% of input (I) and the relative flowthrough (F) material of the Scramble RNA was also loaded in the gel.

The displayed data is the representative image of one of the three biological experiments performed.

Supplementary Figure 4. A) Number of total interactors identified for each RNA fragment (labeled with the letter "F" follow by a number) and definition of the interaction partners in common with the control "Scramble" (green) compared to the protein identified uniquely with SARS-CoV-2 RNA (pink). **B)** Volcano plots of the RaPID-MS analysis of each fragment against the Scramble control. Proteins statistically significant according to the student T-test ($P < 0.05$) are displayed in the figures. Volcano plots of the RaPID-MS analysis of each fragment against the Scramble control. Proteins statistically significant according to the student T-test ($P < 0.05$) are displayed in the figures.

Supplementary Figure 5. A) Venn diagram showing the overlap of the generated RaPID-MS dataset and the previously published dataset on the interactions between SARS-CoV-2 RNA and the host proteins in human cells. **B)** List of the common interactors of RaPID-MS dataset with at least one of the published datasets. **C)** Gene Ontology (GO) analysis performed on the 73 proteins specifically associated with the 10 SARS-CoV-2 RNA fragments and identified by RaPID-MS.

Supplementary Figure 6. A) Scatter chart of the analysed RBPs ranked according to their relative log2 *cat*RAPID score, displaying each RNA fragment at time. **B)** Boxplot representation of the distribution of the predicted interactions according to the log2 *cat*RAPID score.

Supplementary Figure 7.

Nanocompore plots for each reference canonical sgRNA in every cell line. On the y-axis is displayed the GMM p-value, while on the x-axis the log odds ratio (LOR). Thresholds are displayed through red dashed lines. Every point represents a k-mer identified as significant compared to the IVT sample. Of these significant k-mers, those containing the UNUAR motif have been labeled. The color code represents k-mers overlapping with RaPID fragments.

Supplementary Figure 8.

Distributions of Dwell time and median intensity distribution per position for the eight significant sites, shared between at least two cell lines and containing the UGUAR motif. Each position displays distributions for two conditions, the reference (in this case the IVT) and the test condition.

Supplementary Table 1: DNA sequences of the SARS-CoV-2 fragments used in this study.

Supplementary Table 2: Library of 2064 human RNA-binding proteins used in the analyses.

Supplementary Table 3: List of the proteins identified in association with each fragment by RaPID-MS analysis. The protein interactors for each fragment are reported in an independent spreadsheet named with the respective SARS-CoV-2 fragment. The spreadsheet named "Summary" displayed a summary of only the significant interactors identified, according to the T-Test analysis. In addition, it was indicated if proteins were annotated as RNA binding proteins (RBPs) and if they were interacting with only one of the 10 RNA fragments. The spreadsheet named "Overlap published datasets" displayed all the identified proteins and the significant proteins identified in the RaPID-MS dataset and in the published datasets.

Supplementary Table 4: catRAPID performances on RAPID-RBP dataset. For each protein-RNA pair, the catRAPID predictive score, the median LFQ value, the abundance and length of the protein and the normalized LFQ values are shown. Both the overall interactome and the single fragments interactomes are available. The list of proteins with a log2 catRAPID score higher than 5.22 (85th percentile) removing those enriched with Scramble RNA is provided in the datasheet named "85th percentile no scramble". The datasheet named "statistics" contains the Chi squared test applied on the distribution of the *cat*RAPID score of each RNA-protein interaction for each SARS-CoV-2 RNA fragment.

Supplementary Table 5, 6, 7: Modification sites in SARS-CoV-2 infected CaCo-2, CaLu-3 and Vero E6 cells.

- Sheet *samples* - List of samples for the cell line of interest and analysis parameters.
- Sheet *all_significant_sites* - All k-mers passing LOR and GMM p-value thresholds (k-mers overlapping IVT or ORF junctions are not excluded).
- Sheet *all_canonical_Us_sign_sites* - K-mers passing LOR and GMM p-value thresholds with at least one uridine nucleotide and belonging to a canonical sgRNA (k-mers overlapping IVT or ORF junctions are excluded).
- Sheet *5p_significant_sites* - K-mers passing LOR and GMM p-value thresholds located before genomic position 100 (k-mers overlapping IVT or ORF junctions are not excluded).
- Sheet *5p_canonical_Us_sign_sites* - K-mers passing LOR and GMM p-value thresholds with at least one uridine nucleotide, belonging to a canonical sgRNA and

located before genomic position 100 (k-mers overlapping IVT or ORF junctions are not excluded).

- Sheet *Fleming_redundant_all_sites* - All k-mers overlapping one of the Fleming et al. sites according to our analysis (k-mers overlapping IVT or ORF junctions are not excluded).
- Sheet *Fleming_redundant_sign_sites* - K-mers passing LOR and GMM p-value thresholds overlapping one of the Fleming et al. sites according to our analysis (k-mers overlapping IVT or ORF junctions are not excluded).
- Sheet *Fleming_non_red_CandNC_sites* - Non-redundant k-mers passing LOR and GMM p-value thresholds overlapping one of the Fleming et al. sites according to our analysis (k-mers overlapping IVT or ORF junctions are not excluded).
- Sheet *Fleming_non_red_CandN_all_sites* - Non-redundant k-mers overlapping one of the Fleming et al. sites according to our analysis (k-mers overlapping IVT or ORF junctions are not excluded).
- Sheet *peakcalled_canonical_Us* - K-mers passing LOR and GMM p-value thresholds with at least one uridine nucleotide, peakcalled as in Leger et al.(36) and belonging to a canonical sgRNA (k-mers overlapping IVT or ORF junctions are excluded).
- Sheet *Fleming_in_peakcalled_canonical* - K-mers passing LOR and GMM p-value thresholds with at least one uridine nucleotide, peakcalled as in Leger et al.(36), belonging to a canonical sgRNA and overlapping one of the Fleming et al. sites (k-mers overlapping IVT or ORF junctions are excluded).

Supplementary Table 8: Modification sites shared between the different cell lines.

- Sheet *shared_2_U* - modified sites shared between at least two cell lines.
- Sheet *shared_3_U* - modified sites shared between all the three cell lines.

References

1. Mistry,P., Barmania,F., Mellet,J., Peta,K., Strydom,A., Viljoen,I.M., James,W., Gordon,S. and Pepper,M.S. (2022) SARS-CoV-2 Variants, Vaccines, and Host Immunity. *Front. Immunol.*, **12**, 809244. https://doi.org/10.3389/fimmu.2021.809244

2. Coronaviridae Study Group of the International Committee on Taxonomy of Viruses (2020) The species Severe acute respiratory syndrome-related coronavirus: classifying 2019-nCoV and naming it SARS-CoV-2. *Nat. Microbiol.*, **5**, 536–544. https://doi.org/10.1038/s41564-020-0695-z

3. Harrison,A.G., Lin,T. and Wang,P. (2020) Mechanisms of SARS-CoV-2 Transmission and Pathogenesis. *Trends Immunol.*, **41**, 1100–1115. https://doi.org/10.1016/j.it.2020.10.004

4. Zhang,Y.-Z. and Holmes,E.C. (2020) A Genomic Perspective on the Origin and Emergence of SARS-CoV-2. *Cell*, **181**, 223–227. https://doi.org/10.1016/j.cell.2020.03.035

5. Malone,B., Urakova,N., Snijder,E.J. and Campbell,E.A. (2022) Structures and functions of coronavirus replication–transcription complexes and their relevance for SARS-CoV-2 drug design. *Nat. Rev. Mol. Cell Biol.*, **23**, 21–39. https://doi.org/10.1038/s41580-021-00432-z

6. Ugolini,C., Mulroney,L., Leger,A., Castelli,M., Criscuolo,E., Williamson,M.K., Davidson,A.D., Almuqrin,A., Giambruno,R., Jain,M., *et al.* (2022) Nanopore ReCappable sequencing maps SARS-CoV-2 *5′* capping sites and provides new insights into the structure of sgRNAs. *Nucleic Acids Res.*, **50**, 3475–3489. https://doi.org/10.1093/nar/gkac144

7. Sola,I., Almazán,F., Zúñiga,S. and Enjuanes,L. (2015) Continuous and Discontinuous RNA Synthesis in Coronaviruses. *Annu. Rev. Virol.*, **2**, 265–288. https://doi.org/10.1146/annurev-virology-100114-055218

8. Banerjee,A.K., Blanco,M.R., Bruce,E.A., Honson,D.D., Chen,L.M., Chow,A., Bhat,P., Ollikainen,N., Quinodoz,S.A., Loney,C., *et al.* (2020) SARS-CoV-2 Disrupts Splicing, Translation, and Protein Trafficking to Suppress Host Defenses. *Cell*, **183**, 1325-1339.e21. https://doi.org/10.1016/j.cell.2020.10.004

9. Yin,X., Riva,L., Pu,Y., Martin-Sancho,L., Kanamune,J., Yamamoto,Y., Sakai,K., Gotoh,S., Miorin,L., De Jesus,P.D., *et al.* (2021) MDA5 Governs the Innate Immune Response to SARS-CoV-2 in Lung Epithelial Cells. *Cell Rep.*, **34**, 108628. https://doi.org/10.1016/j.celrep.2020.108628

10. Li,N., Hui,H., Bray,B., Gonzalez,G.M., Zeller,M., Anderson,K.G., Knight,R., Smith,D., Wang,Y., Carlin,A.F., *et al.* (2021) METTL3 regulates viral m6A RNA modification and host cell innate immune responses during SARS-CoV-2 infection. *Cell Rep.*, **35**, 109091.

https://doi.org/10.1016/j.celrep.2021.109091

11. Kim,Y.-M. and Shin,E.-C. (2021) Type I and III interferon responses in SARS-CoV-2 infection. *Exp. Mol. Med.*, **53**, 750–760. https://doi.org/10.1038/s12276-021-00592-0

12. Kamel,W., Noerenberg,M., Cerikan,B., Chen,H., Järvelin,A.I., Kammoun,M., Lee,J.Y., Shuai,N., Garcia-Moreno,M., Andrejeva,A., *et al.* (2021) Global analysis of protein-RNA interactions in SARS-CoV-2-infected cells reveals key regulators of infection. *Mol. Cell*, **81**, 2851-2867.e7. https://doi.org/10.1016/j.molcel.2021.05.023

13. Lee,S., Lee,Y., Choi,Y., Son,A., Park,Y., Lee,K.-M., Kim,J., Kim,J.-S. and Kim,V.N. (2021) The SARS-CoV-2 RNA interactome. *Mol. Cell*, **81**, 2838-2850.e6. https://doi.org/10.1016/j.molcel.2021.04.022

14. Flynn,R.A., Belk,J.A., Qi,Y., Yasumoto,Y., Wei,J., Alfajaro,M.M., Shi,Q., Mumbach,M.R., Limaye,A., DeWeirdt,P.C., *et al.* (2021) Discovery and functional interrogation of SARS-CoV-2 RNA-host protein interactions. *Cell*, **184**, 2394-2411.e16. https://doi.org/10.1016/j.cell.2021.03.012

15. Schmidt,N., Lareau,C.A., Keshishian,H., Ganskih,S., Schneider,C., Hennig,T., Melanson,R., Werner,S., Wei,Y., Zimmer,M., *et al.* (2021) The SARS-CoV-2 RNA–protein interactome in infected human cells. *Nat. Microbiol.*, **6**, 339–353. https://doi.org/10.1038/s41564-020-00846-z

16. Lei,X., Dong,X., Ma,R., Wang,W., Xiao,X., Tian,Z., Wang,C., Wang,Y., Li,L., Ren,L., *et al.* (2020) Activation and evasion of type I interferon responses by SARS-CoV-2. *Nat. Commun.*, **11**, 3810. https://doi.org/10.1038/s41467-020-17665-9

17. Xia,H., Cao,Z., Xie,X., Zhang,X., Chen,J.Y.-C., Wang,H., Menachery,V.D., Rajsbaum,R. and Shi,P.-Y. (2020) Evasion of Type I Interferon by SARS-CoV-2. *Cell Rep.*, **33**, 108234. https://doi.org/10.1016/j.celrep.2020.108234

18. Vandelli,A., Monti,M., Milanetti,E., Armaos,A., Rupert,J., Zacco,E., Bechara,E., Delli Ponti,R. and Tartaglia,G.G. (2020) Structural analysis of SARS-CoV-2 genome and predictions of the human interactome. *Nucleic Acids Res.*, **48**, 11270–11283. https://doi.org/10.1093/nar/gkaa864

19. Ramanathan,M., Majzoub,K., Rao,D.S., Neela,P.H., Zarnegar,B.J., Mondal,S., Roth,J.G., Gai,H., Kovalski,J.R., Siprashvili,Z., *et al.* (2018) RNA–protein interaction detection in living cells. *Nat. Methods*, **15**, 207–212. https://doi.org/10.1038/nmeth.4601

20. Sanchez de Groot,N., Armaos,A., Graña-Montes,R., Alriquet,M., Calloni,G., Vabulas,R.M. and Tartaglia,G.G. (2019) RNA structure drives interaction with

proteins. *Nat. Commun.*, **10**, 3246.
https://doi.org/10.1038/s41467-019-10923-5

21. Cerase,A., Calabrese,J.M. and Tartaglia,G.G. (2022) Phase separation drives X-chromosome inactivation. *Nat. Struct. Mol. Biol.*, **29**, 183–185.
https://doi.org/10.1038/s41594-021-00697-0

22. Vandelli,A., Vocino,G. and Tartaglia,G.G. (2022) Phase Separation Drives SARS-CoV-2 Replication: A Hypothesis. *Front. Mol. Biosci.*, **9**, 893067.
https://doi.org/10.3389/fmolb.2022.893067

23. Schubert,K., Karousis,E.D., Jomaa,A., Scaiola,A., Echeverria,B., Gurzeler,L.-A., Leibundgut,M., Thiel,V., Mühlemann,O. and Ban,N. (2020) SARS-CoV-2 Nsp1 binds the ribosomal mRNA channel to inhibit translation. *Nat. Struct. Mol. Biol.*, **27**, 959–966.
https://doi.org/10.1038/s41594-020-0511-8

24. Brant,A.C., Tian,W., Majerciak,V., Yang,W. and Zheng,Z.-M. (2021) SARS-CoV-2: from its discovery to genome structure, transcription, and replication. *Cell Biosci.*, **11**, 136.
https://doi.org/10.1186/s13578-021-00643-z

25. Armaos,A., Colantoni,A., Proietti,G., Rupert,J. and Tartaglia,G.G. (2021) *cat* RAPID *omics v2.0* : going deeper and wider in the prediction of protein–RNA interactions. *Nucleic Acids Res.*, **49**, W72–W79.
https://doi.org/10.1093/nar/gkab393

26. Cid-Samper,F., Gelabert-Baldrich,M., Lang,B., Lorenzo-Gotor,N., Ponti,R.D., Severijnen,L.-A.W.F.M., Bolognesi,B., Gelpi,E., Hukema,R.K., Botta-Orfila,T., *et al.* (2018) An Integrative Study of Protein-RNA Condensates Identifies Scaffolding RNAs and Reveals Players in Fragile X-Associated Tremor/Ataxia Syndrome. *Cell Rep.*, **25**, 3422-3434.e7.
https://doi.org/10.1016/j.celrep.2018.11.076

27. Agostini,F., Cirillo,D., Bolognesi,B. and Tartaglia,G.G. (2013) X-inactivation: quantitative predictions of protein interactions in the Xist network. *Nucleic Acids Res.*, **41**, e31–e31.
https://doi.org/10.1093/nar/gks968

28. Armaos,A., Zacco,E., Sanchez de Groot,N. and Tartaglia,G.G. (2021) RNA-protein interactions: Central players in coordination of regulatory networks. *BioEssays*, **43**, 2000118.
https://doi.org/10.1002/bies.202000118

29. Ramanathan,M., Majzoub,K., Rao,D.S., Neela,P.H., Zarnegar,B.J., Mondal,S., Roth,J.G., Gai,H., Kovalski,J.R., Siprashvili,Z., *et al.* (2018) RNA–protein interaction detection in living cells. *Nat. Methods*, **15**, 207–212.
https://doi.org/10.1038/nmeth.4601

30. Iselin,L., Palmalux,N., Kamel,W., Simmonds,P., Mohammed,S. and Castello,A. (2022)

Uncovering viral RNA–host cell interactions on a proteome-wide scale. *Trends Biochem. Sci.*, **47**, 23–38.
https://doi.org/10.1016/j.tibs.2021.08.002

31. Edwards,J.M., Long,J., de Moor,C.H., Emsley,J. and Searle,M.S. (2013) Structural insights into the targeting of mRNA GU-rich elements by the three RRMs of CELF1. *Nucleic Acids Res.*, **41**, 7153–7166.
https://doi.org/10.1093/nar/gkt470
http://www.ncbi.nlm.nih.gov/pmc/articles/PMC3737555

32. Baggen,J., Vanstreels,E., Jansen,S. and Daelemans,D. (2021) Cellular host factors for SARS-CoV-2 infection. *Nat. Microbiol.*, **6**, 1219–1232.
https://doi.org/10.1038/s41564-021-00958-0

33. Ziv,O., Price,J., Shalamova,L., Kamenova,T., Goodfellow,I., Weber,F. and Miska,E.A. (2020) The Short- and Long-Range RNA-RNA Interactome of SARS-CoV-2. *Mol. Cell*, **80**, 1067-1077.e5.
https://doi.org/10.1016/j.molcel.2020.11.004

34. Horlacher,M., Oleshko,S., Hu,Y., Ghanbari,M., Cantini,G., Schinke,P., Vergara,E.E., Bittner,F., Mueller,N.S., Ohler,U., *et al.* (2021) Computational Mapping of the Human-SARS-CoV-2 Protein-RNA Interactome Bioinformatics.
https://doi.org/10.1101/2021.12.22.472458

35. Akbari,B., Ahmadi,E., Zamir,M.R., Shaker,M.S. and Noorbakhsh,F. (2022) SARS-CoV-2 Helicase might interfere with cellular nonsense-mediated RNA decay, insights from a bioinformatics study Bioinformatics.
https://doi.org/10.1101/2022.05.30.494036

36. Leger,A., Amaral,P.P., Pandolfini,L., Capitanchik,C., Capraro,F., Miano,V., Migliori,V., Toolan-Kerr,P., Sideri,T., Enright,A.J., *et al.* (2021) RNA modifications detection by comparative Nanopore direct RNA sequencing. *Nat. Commun.*, **12**, 7198.
https://doi.org/10.1038/s41467-021-27393-3

37. Kim,D., Lee,J.-Y., Yang,J.-S., Kim,J.W., Kim,V.N. and Chang,H. (2020) The Architecture of SARS-CoV-2 Transcriptome. *Cell*, **181**, 914-921.e10.
https://doi.org/10.1016/j.cell.2020.04.011

38. Simpson,J.T., Workman,R.E., Zuzarte,P.C., David,M., Dursi,L.J. and Timp,W. (2017) Detecting DNA cytosine methylation using nanopore sequencing. *Nat. Methods*, **14**, 407–410.
https://doi.org/10.1038/nmeth.4184

39. Fleming,A.M., Mathewson,N.J., Howpay Manage,S.A. and Burrows,C.J. (2021) Nanopore Dwell Time Analysis Permits Sequencing and Conformational Assignment of Pseudouridine in SARS-CoV-2. *ACS Cent. Sci.*, **7**, 1707–1717.
https://doi.org/10.1021/acscentsci.1c00788

40. Onomoto,K., Yoneyama,M., Fung,G., Kato,H. and Fujita,T. (2014) Antiviral innate immunity and stress granule responses. *Trends Immunol.*, **35**, 420–428.

https://doi.org/10.1016/j.it.2014.07.006

41. Izadpanah,A., Rappaport,J. and Datta,P.K. (2022) Epitranscriptomics of SARS-CoV-2 Infection. *Front. Cell Dev. Biol.*, **10**, 849298. https://doi.org/10.3389/fcell.2022.849298

42. Burgess,H.M., Depledge,D.P., Thompson,L., Srinivas,K.P., Grande,R.C., Vink,E.I., Abebe,J.S., Blackaby,W.P., Hendrick,A., Albertella,M.R., *et al.* (2021) Targeting the m ^{6} A RNA modification pathway blocks SARS-CoV-2 and HCoV-OC43 replication. *Genes Dev.*, **35**, 1005–1019. https://doi.org/10.1101/gad.348320.121

43. Leppek,K., Byeon,G.W., Kladwang,W., Wayment-Steele,H.K., Kerr,C.H., Xu,A.F., Kim,D.S., Topkar,V.V., Choe,C., Rothschild,D., *et al.* (2022) Combinatorial optimization of mRNA structure, stability, and translation for RNA-based therapeutics. *Nat. Commun.*, **13**, 1536. https://doi.org/10.1038/s41467-022-28776-w

44. Workman,R.E., Tang,A.D., Tang,P.S., Jain,M., Tyson,J.R., Razaghi,R., Zuzarte,P.C., Gilpatrick,T., Payne,A., Quick,J., *et al.* (2019) Nanopore native RNA sequencing of a human poly(A) transcriptome. *Nat. Methods*, **16**, 1297–1305. https://doi.org/10.1038/s41592-019-0617-2

45. Purchal,M.K., Eyler,D.E., Tardu,M., Franco,M.K., Korn,M.M., Khan,T., McNassor,R., Giles,R., Lev,K., Sharma,H., *et al.* (2022) Pseudouridine synthase 7 is an opportunistic enzyme that binds and modifies substrates with diverse sequences and structures. *Proc. Natl. Acad. Sci.*, **119**, e2109708119. https://doi.org/10.1073/pnas.2109708119

46. Bellucci,M., Agostini,F., Masin,M. and Tartaglia,G.G. (2011) Predicting protein associations with long noncoding RNAs. *Nat. Methods*, **8**, 444–445. https://doi.org/10.1038/nmeth.1611

47. Shevchenko,A., Tomas,H., Havli,J., Olsen,J.V. and Mann,M. (2006) In-gel digestion for mass spectrometric characterization of proteins and proteomes. *Nat. Protoc.*, **1**, 2856–2860. https://doi.org/10.1038/nprot.2006.468

48. Cox,J., Hein,M.Y., Luber,C.A., Paron,I., Nagaraj,N. and Mann,M. (2014) Accurate Proteome-wide Label-free Quantification by Delayed Normalization and Maximal Peptide Ratio Extraction, Termed MaxLFQ. *Mol. Cell. Proteomics*, **13**, 2513–2526. https://doi.org/10.1074/mcp.M113.031591

49. Cox,J. and Mann,M. (2008) MaxQuant enables high peptide identification rates, individualized p.p.b.-range mass accuracies and proteome-wide protein quantification. *Nat. Biotechnol.*, **26**, 1367–1372. https://doi.org/10.1038/nbt.1511

50. Tyanova,S., Temu,T., Sinitcyn,P., Carlson,A., Hein,M.Y., Geiger,T., Mann,M. and Cox,J.

(2016) The Perseus computational platform for comprehensive analysis of (prote)omics data. *Nat. Methods*, **13**, 731–740.
https://doi.org/10.1038/nmeth.3901

51. Su,G., Morris,J.H., Demchak,B. and Bader,G.D. (2014) Biological Network Exploration with Cytoscape 3. *Curr. Protoc. Bioinforma.*, **47**.
https://doi.org/10.1002/0471250953.bi0813s47

52. Kerpedjiev,P., Hammer,S. and Hofacker,I.L. (2015) Forna (force-directed RNA): Simple and effective online RNA secondary structure diagrams. *Bioinformatics*, **31**, 3377–3379.
https://doi.org/10.1093/bioinformatics/btv372

53. Huang,D.W., Sherman,B.T. and Lempicki,R.A. (2009) Systematic and integrative analysis of large gene lists using DAVID bioinformatics resources. *Nat. Protoc.*, **4**, 44–57.
https://doi.org/10.1038/nprot.2008.211

54. Lang,B., Armaos,A. and Tartaglia,G.G. (2019) RNAct: Protein–RNA interaction predictions for model organisms with supporting experimental data. *Nucleic Acids Res.*, **47**, D601–D606.
https://doi.org/10.1093/nar/gky967

55. Wang,M., Herrmann,C.J., Simonovic,M., Szklarczyk,D. and Mering,C. (2015) Version 4.0 of PaxDb: Protein abundance data, integrated across model organisms, tissues, and cell-lines. *PROTEOMICS*, **15**, 3163–3168.
https://doi.org/10.1002/pmic.201400441

56. The UniProt Consortium, Bateman,A., Martin,M.-J., Orchard,S., Magrane,M., Agivetova,R., Ahmad,S., Alpi,E., Bowler-Barnett,E.H., Britto,R., *et al.* (2021) UniProt: the universal protein knowledgebase in 2021. *Nucleic Acids Res.*, **49**, D480–D489.
https://doi.org/10.1093/nar/gkaa1100

57. Gamaarachchi,H., Lam,C.W., Jayatilaka,G., Samarakoon,H., Simpson,J.T., Smith,M.A. and Parameswaran,S. (2020) GPU accelerated adaptive banded event alignment for rapid comparative nanopore signal analysis. *BMC Bioinformatics*, **21**, 343.
https://doi.org/10.1186/s12859-020-03697-x

58. Li,H. (2018) Minimap2: pairwise alignment for nucleotide sequences. *Bioinforma. Oxf. Engl.*, **34**, 3094–3100.
https://doi.org/10.1093/bioinformatics/bty191
http://www.ncbi.nlm.nih.gov/pmc/articles/PMC6137996

59. Virtanen,P., Gommers,R., Oliphant,T.E., Haberland,M., Reddy,T., Cournapeau,D., Burovski,E., Peterson,P., Weckesser,W., Bright,J., *et al.* (2020) SciPy 1.0: fundamental algorithms for scientific computing in Python. *Nat. Methods*, **17**, 261–272.
https://doi.org/10.1038/s41592-019-0686-2

60. Kent,W.J., Sugnet,C.W., Furey,T.S., Roskin,K.M., Pringle,T.H., Zahler,A.M. and Haussler, and D. (2002) The Human Genome Browser at UCSC. *Genome Res.*, **12**, 996–1006. https://doi.org/10.1101/gr.229102

61. Perez-Riverol,Y., Bai,J., Bandla,C., García-Seisdedos,D., Hewapathirana,S., Kamatchinathan,S., Kundu,D.J., Prakash,A., Frericks-Zipper,A., Eisenacher,M., *et al.* (2022) The PRIDE database resources in 2022: a hub for mass spectrometry-based proteomics evidences. *Nucleic Acids Res.*, **50**, D543–D552. https://doi.org/10.1093/nar/gkab1038

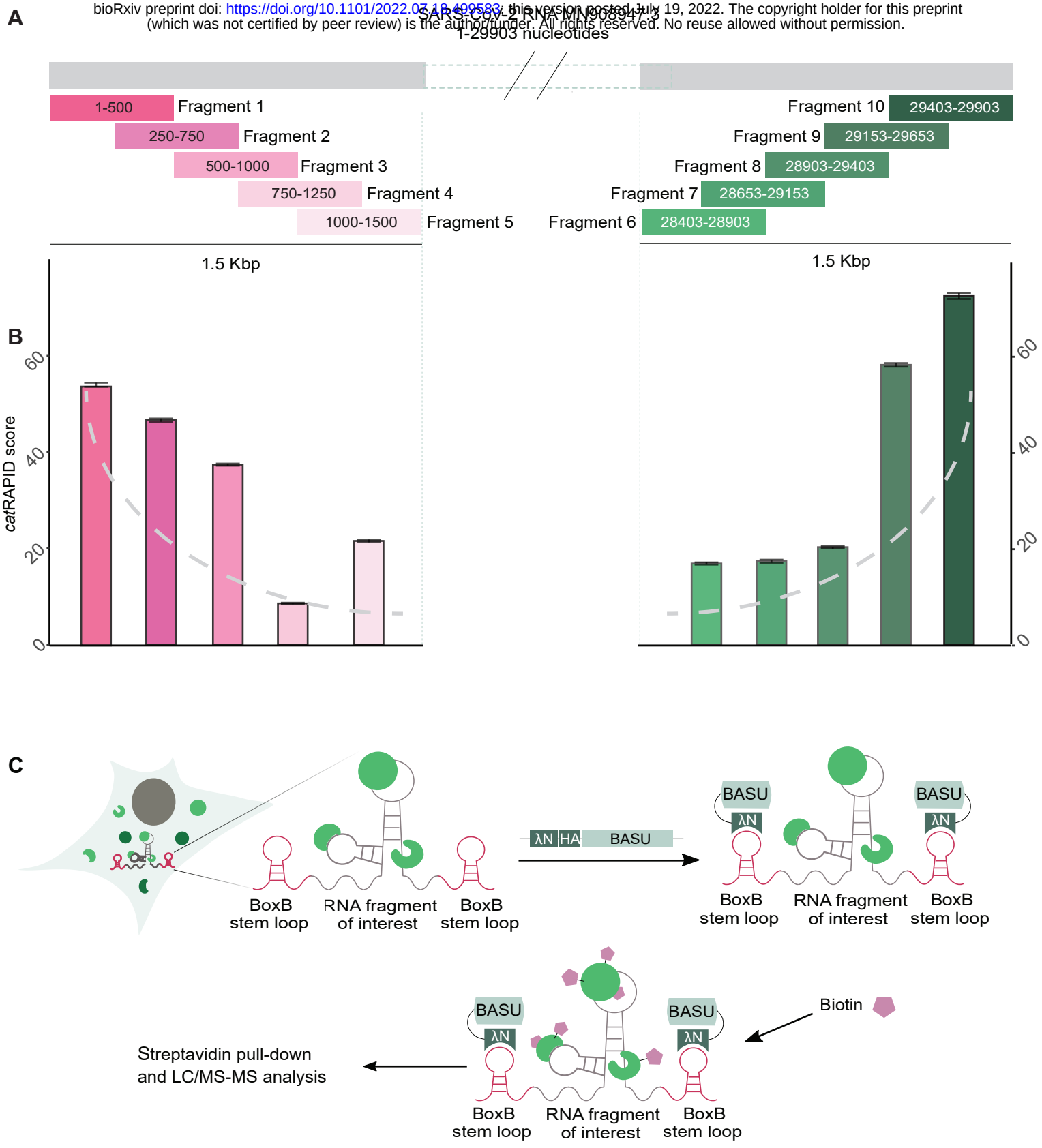

Figure 1.

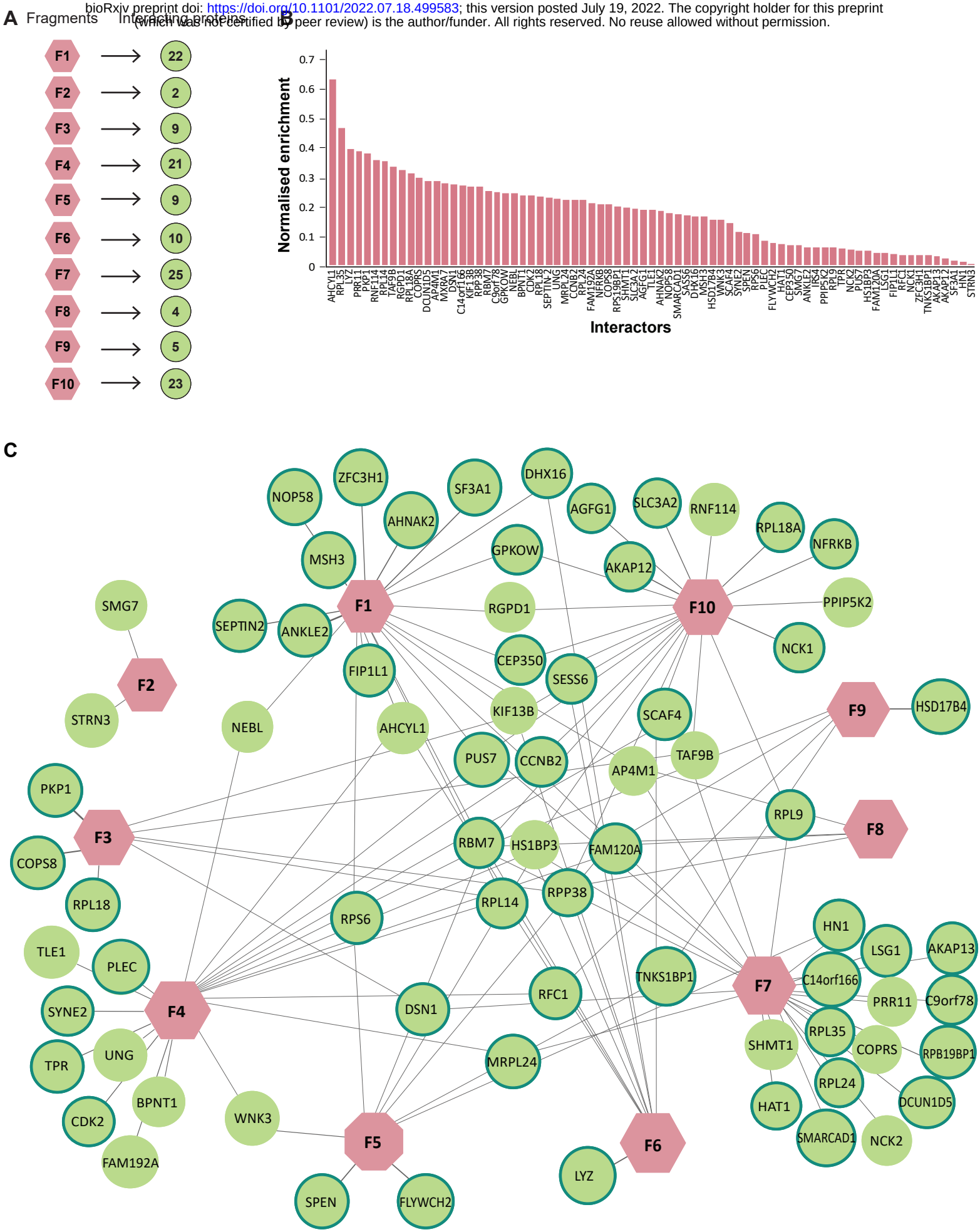

Figure 2.

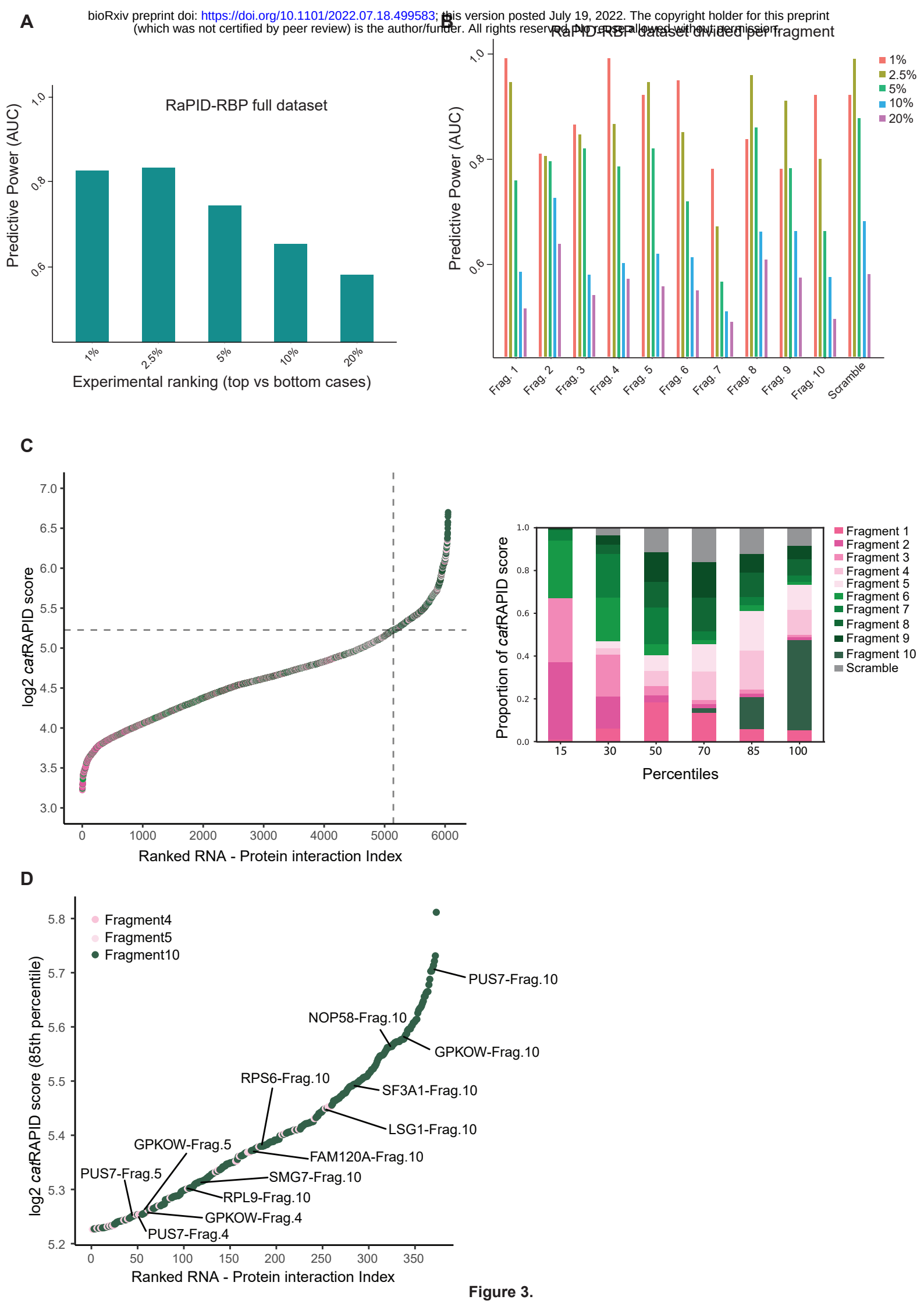

Figure 3.

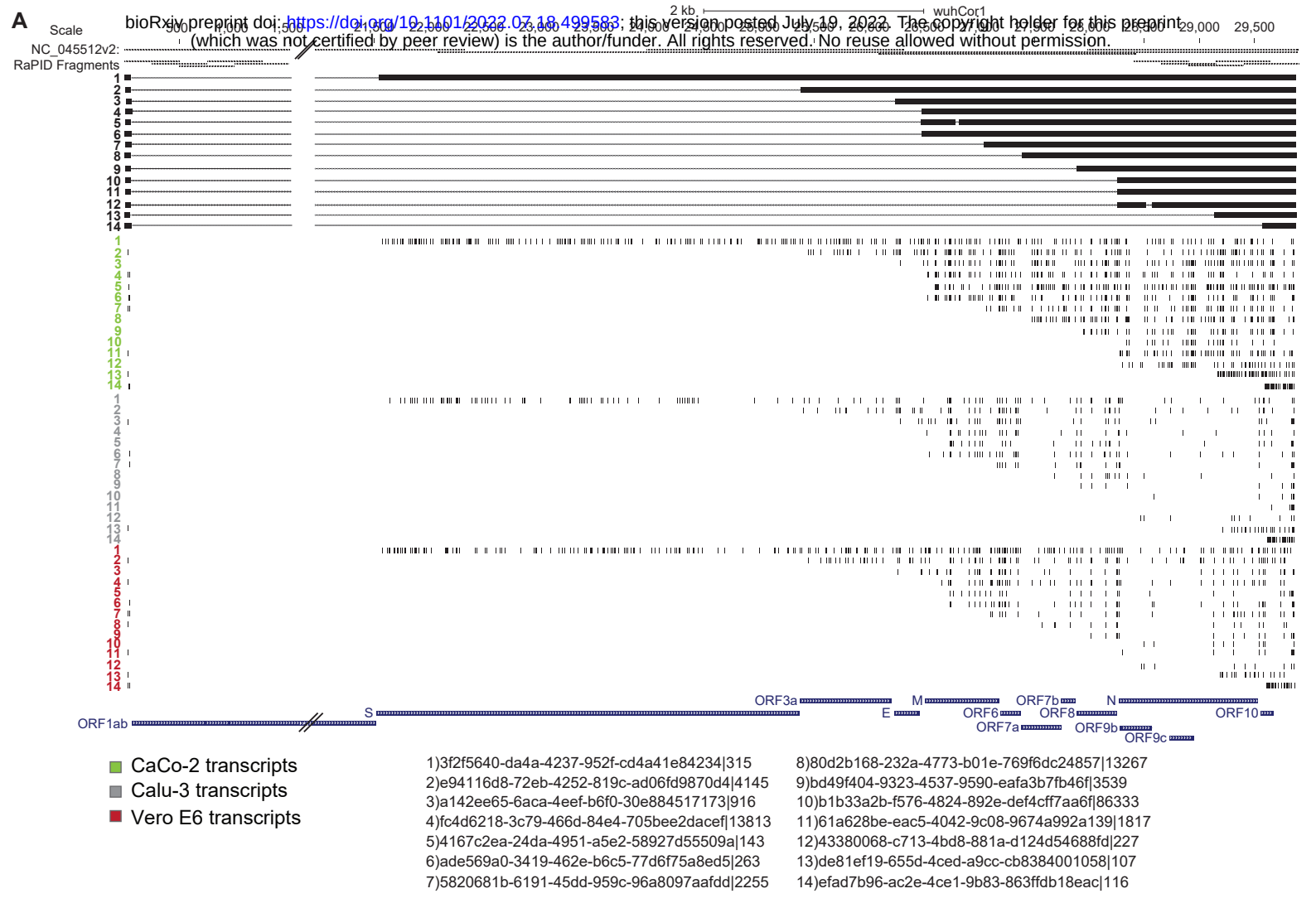

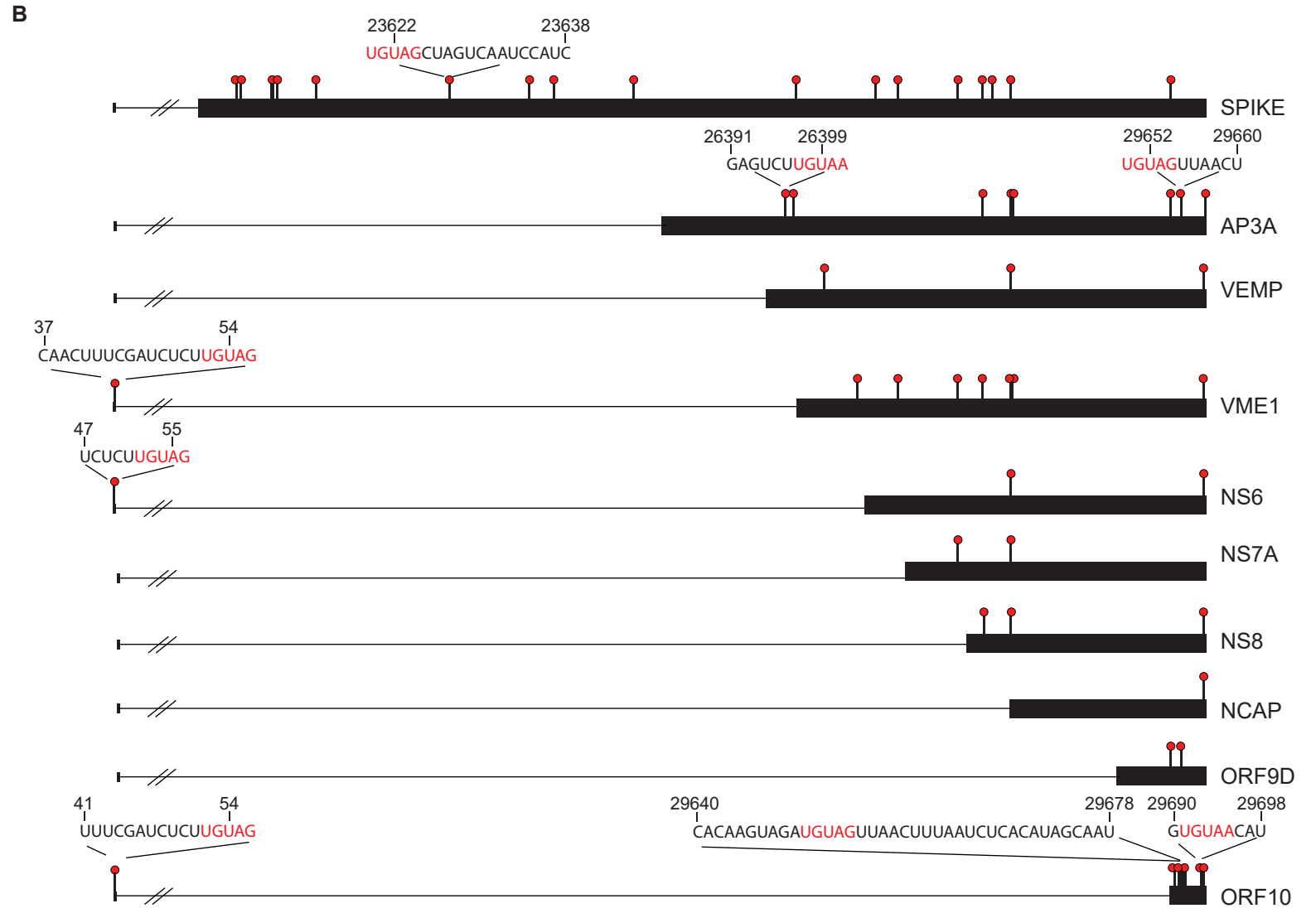

Figure 4.